

Highly-efficient generation of coherent light at 2128 nm via degenerate optical-parametric oscillation

CHRISTIAN DARSOW-FROMM¹, MAIK SCHRÖDER¹, JULIAN GURS^{1,2}, ROMAN SCHNABEL¹, AND SEBASTIAN STEINLECHNER^{3,4}

¹Institut für Laserphysik und Zentrum für Optische Quantentechnologien der Universität Hamburg, Luruper Chaussee 149, 22761 Hamburg, Germany

²3rd Institute of Physics, University of Stuttgart and Institute for Quantum Science and Technology IQST, 70569, Stuttgart, Germany

³Faculty of Science and Engineering, Maastricht University, Duboisdomein 30, 6229 GT Maastricht, The Netherlands

⁴Nikhef, Science Park 105, 1098 XG Amsterdam, The Netherlands

Compiled August 20, 2020

Cryogenic operation in conjunction with new test-mass materials promises to reduce the sensitivity limitations from thermal noise in gravitational-wave detectors. The currently most advanced materials under discussion are crystalline silicon as a substrate with amorphous silicon-based coatings. They require, however, operational wavelengths around 2 μm to avoid laser absorption. Here, we present a light source at 2128 nm based on a degenerate optical parametric oscillator (DOPO) to convert light from a 1064 nm non-planar ring-oscillator (NPRO). We achieve an external conversion efficiency of $(88.3 \pm 1.4) \%$ at a pump power of 52 mW in PPKTP (periodically-poled potassium titanyl phosphate, internal efficiency was 94 %), from which we infer an effective non-linearity of $(4.75 \pm 0.18) \text{ pm/V}$. With our approach, light from the established and existing laser sources can be efficiently converted to the 2 μm regime, while retaining the excellent stability properties. © 2020 Optical Society of America

<http://dx.doi.org/10.1364/ao.XX.XXXXXX>

1. INTRODUCTION

Since the observation of the first black-hole coalescence in 2015, gravitational-wave detection has evolved from proof-of-principle experiments into the new field of gravitational-wave astronomy [1–3]. Further increasing the sensitivity of detectors not only allows the observation of weaker signals, but will also expand the detection range towards the entire universe. This promises new insights into cosmology and even the origin of the universe by statistical evaluation of the gravitational-wave background [4]. Especially the low-frequency regime is of interest in the context of multi-messenger astronomy, since merger events cross the gravitational-wave spectrum days to weeks before the coalescence, giving ample pre-warning for a precise sky localization of any electro-magnetic counterpart.

Enhancement of the detector sensitivity, however, is a highly complex task involving many fields of expertise. For instance, coating thermal noise poses a significant limitation of current detectors, particularly in the mid-frequency range from several tens of Hz to a few hundreds of Hz [5–7]. This will be solved by operation at cryogenic temperatures and a simultaneous change of the mirror substrate and coating materials. The most promising substrate candidate, crystalline silicon, excels with high mechanical Q-factor and thermal conductivity in the cryogenic regime, in contrast to the currently used fused silica [8, 9]. Latest research in coating technology, on the other hand, has shown promising mechanical loss results with amorphous silicon thin films [10]. Optimized coatings utilizing this material could show a thermal noise that is a factor of twelve below conventional silica-tantala

coatings [11]. However, the operation wavelength with these novel coatings is restricted to above 1.8 μm . Otherwise the absorption would exceed the required order of a few ppm [9, 12, 13], which would lead to significant heating of the test masses, distortions from thermal lensing and hinder advanced quantum sensing techniques. As such, design studies for upcoming detector generations such as LIGO Voyager and Cosmic Explorer [12] feature wavelengths around 2 μm . Prototype facilities like ETpathfinder [14] are planning to investigate interferometry with this novel wavelength for gravitational-wave detection.

New laser schemes have to provide a comprehensive solution for high precision quantum metrology, including optics and detection devices [15–18]. In addition, the laser sources themselves have stringent requirements in terms of power stability, amplitude and phase noise, as well as spatial mode quality. It took decades of development effort to reach the technological maturity with laser sources at 1064 nm. Laser technologies at around 2 μm are most often based on either holmium- or thulium-doped laser media, but their maturity and performance levels still leave a lot to be desired [19], as their conventional use in medical and LIDAR applications does not require exceptional stability. In contrast, our approach employs laser sources at 1064 nm currently used in gravitational-wave detection and converts the light via optical parametric down-conversion to 2128 nm. This nonlinear process is known to retain the stability and noise properties of the pump [20, 21], allowing us to fully take advantage of the already optimized technology.

Prior optical parametric oscillators have been used e.g. to provide

tunable continuous-wave laser sources [22], wavelength conversion of pumped lasers [23], or even to generate quantum random bits, exploiting their inherent bistability [24].

Here we report highly efficient generation of coherent light at 2128 nm employing an external degenerate optical parametric oscillator (DOPO) and verify the preservation of power stability, amplitude and phase noise, as well as spatial mode quality.

2. EXPERIMENTAL SETUP

Our setup for the generation of 2128 nm light was based on type 0 degenerate optical-parametric oscillation (DOPO) in a nonlinear resonator, pumped by 1064 nm light from a nonplanar ring oscillator (NPRO) [25] master laser, see figure 1. We chose a hemilithic resonator design around a periodically-poled potassium titanyl phosphate (PP-KTP) crystal, where one side of the crystal functioned as end mirror of the resonator. This side was highly reflective for both wavelengths, while the other side of the crystal was anti-reflective. The coupling mirror was mounted on a piezo to scan and stabilize the cavity length and was coated with a reflectivity of 96% at 1064 nm and 90% at 2128 nm. The overall cavity length has been simulated and optimized to suppress higher-order Gaussian modes. Further optical properties of the DOPO are summarized in table 1. Our cavity was coupled with a mode-matching efficiency of 94%, which was mainly limited by the beam shape of the pump laser. We used a modified Pound-Drever-Hall control scheme in transmission of the resonators together with a digital controller [26] to stabilize the DOPO cavity.

To simultaneously achieve the degeneracy of signal and idler fields, as well as a high conversion efficiency, we precisely controlled the temperature of two regions of the crystal [27, 28]. The main temperature T_1 adjusted the quasi phase-matching for the degenerate process. About 1 mm of the crystal's high-reflective (HR) end was separately tempera-

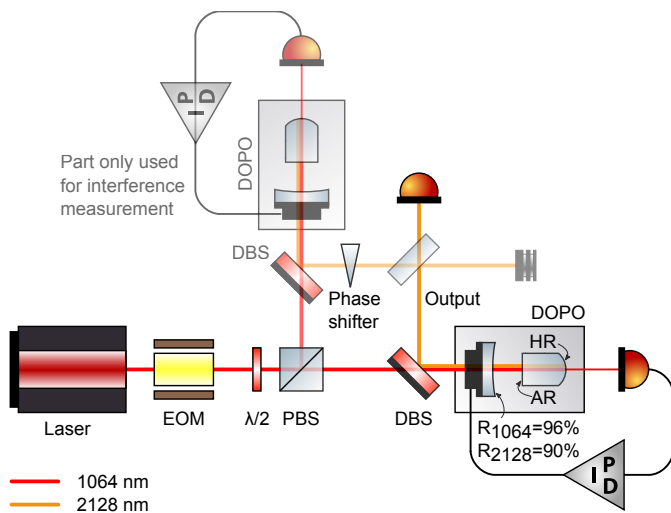


Fig. 1. Simplified schematics of our experiment. The laser was a NPRO with 2 W output power at the wavelength $\lambda = 1064$ nm. An electro-optical modulator (EOM) provided phase-modulation sidebands at 28 MHz for a Pound-Drever-Hall locking scheme of the cavity. A combination of half-waveplate and polarizing beam-splitter (PBS) adjusted the pump power. The converted light was split from the pumping beam with a dichroic beam-splitter (DBS). For diagnostic purposes, the converted light could be sent towards a spectrometer and confocal cavity. A second, identical DOPO was installed together with a phase shifter and 50/50 beam-splitter for the interference measurement (sec. C).

	1064	2128	nm
finesse	153	59.5	
waist radius	33.2	47.4	μm
free spectral range	3.80	3.83	GHz
linewidth (FWHM)	24.9	64.3	MHz
coupler reflectivity	96	90	%

Table 1. Optical properties of the DOPO cavity for the pump and converted wavelengths.

ture controlled (T_2) to ensure resonance for 1064 nm and 2128 nm at the same time.

The 1064 nm and 2128 nm fields were separated from each other by a dichroic beam splitter and the power of the converted light was tracked by a photodiode. To determine the wavelengths of signal and idler fields, we used a Bruker Equinox 55 spectrometer with a resolution of 0.5 cm^{-1} , which corresponds to 0.23 nm at $\lambda = 2128 \text{ nm}$.

DOPOs are known to be highly sensitive to reflection of light back into the resonator [29], which is caused by a bistability allowing the randomly chosen phase states 0 and π for the converted light [21, 24]. For this reason, we tried to avoid back-reflections as much as possible by slightly tilting all optics after the DOPO. In addition, we found an operation above the point of maximum efficiency to be much less sensitive than below this point. An output power of about 80 mW has been shown to be stable for our configuration.

3. RESULTS/CHARACTERIZATION

We characterized our setup to validate the performance required for interferometric light sources in gravitational-wave detection. This includes temperature tuning behavior of the oscillation wavelength, conversion efficiency, interferometric visibility, and power stability. We would have liked to also include an amplitude noise spectrum of the DOPO output field, but were unable to obtain a sufficiently broadband, low-noise and high dynamic range photo detector for $2 \mu\text{m}$.

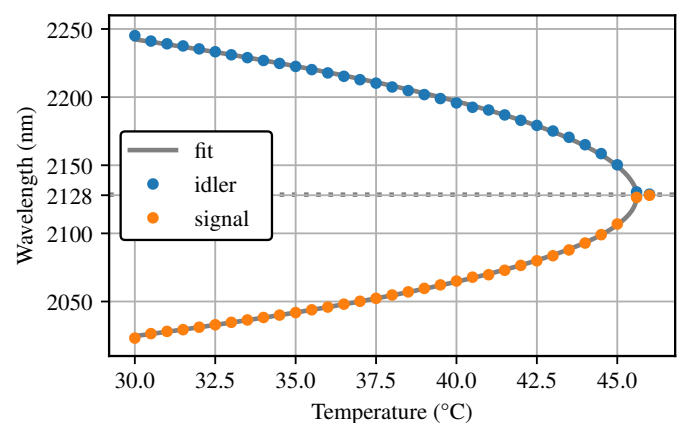


Fig. 2. Measured signal and idler wavelengths versus crystal temperature ($T_1 = T_2$). Below the temperature of degeneracy (about 45.1°C for this crystal) the difference of the signal and idler wavelengths increased with decreasing temperature. In this region the power of the converted light was nearly constant. At degeneracy the output power dropped quickly when the temperature was further increased and the conversion stopped completely at temperatures exceeding 46°C .

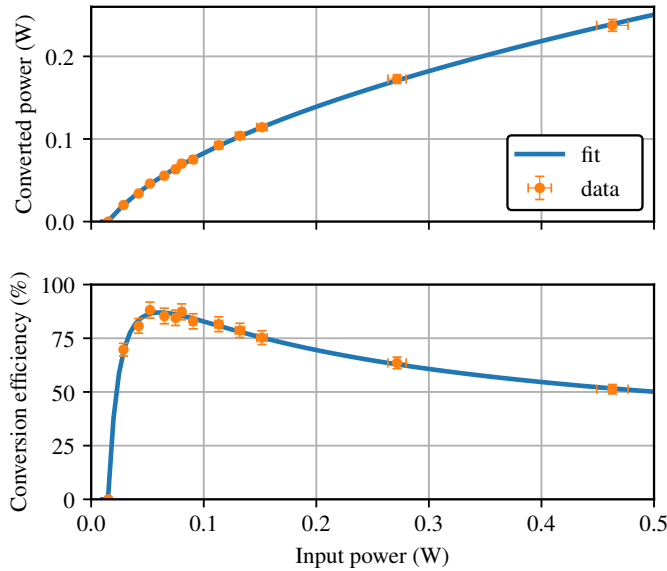


Fig. 3. Power of the converted light (top) and external conversion efficiency (bottom). The indicated error bars correspond to the measurement accuracy of the thermal power meter of 3%. The blue lines show our best fit to the data from a time-domain simulation model. At the point of maximum conversion efficiency, 52 mW of pump power was converted into 46 mW of output power.

A. Wavelength dependency on the crystal temperature

Tuning the crystal temperature T_1 varies the wavelengths of the signal and idler beams, as it influences the phase-matching condition of the nonlinear crystal. The main effect results from the temperature-dependent refractive index, while the thermal expansion has a relatively small contribution [30]. Figure 2 shows the wavelength dependency of signal and idler on the temperature, measured with the spectrometer. Our measurement shows the expected temperature dependency near degeneracy, $\Delta\omega = k\sqrt{T - T_0}$ [31], where $\Delta\omega$ is the difference in frequency between signal and idler. Only in a small temperature region degeneracy could be reached, requiring a fine tuning of the phase-matching temperature.

When increasing the crystal temperature, the output power of the converted light stays roughly constant up to the point of degeneracy. Above this point, the output power quickly dropped as energy conservation and phase matching condition could no longer be satisfied simultaneously.

B. Conversion efficiency

The conversion efficiency η depending on the pump power was measured by inserting a thermal power head into the pump and output fields, respectively. Figure 3 shows the measured power levels and the calculated external conversion efficiency, i.e. not corrected for power loss from mode-matching, reflection loss of the crystal's AR coating, internal absorption, as well as residual transmission through the resonator. We fitted a numerical model to the measured data with the time-domain simulation program NLCS [32]. As free parameters for the simulation, we used the effective non-linearity d_Q and maximum external conversion efficiency η . Here, d_Q is related to the nonlinear coefficient d_{33} of our crystal geometry by an additional Fourier factor introduced by the quasi phase-matching, $d_Q = \frac{2}{\pi}d_{33}$.

We obtained $d_Q = (4.75 \pm 0.18)$ pm/V for the harmonic transition from 1064 nm to 2128 nm in quasi phase-matched PPKTP. The result for the maximum external conversion efficiency was $\eta =$

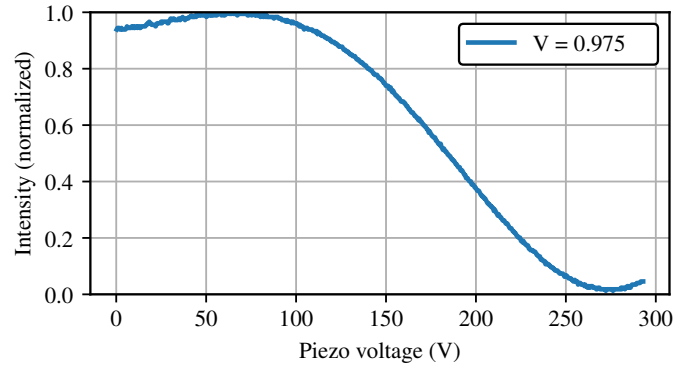


Fig. 4. Demonstration of spatial mode quality and frequency stability. Shown is the interference fringe $V = 0.975$ generated by overlapping two independently generated 2128 nm beams on a 50/50 beam splitter. The phase difference was scanned by applying a high voltage ramp to a piezo-mounted mirror. The achievable phase difference was limited by the travel range of the piezo, compared to the long wavelength.

$(88.3 \pm 1.4)\%$ at an incident pump power of 52 mW. Correcting for the imperfect mode matching of the pump beam, we infer an internal conversion efficiency greater than 94%.

Far above the pump power of optimal conversion of 50 mW, i.e. above 600 mW, the output power at 2128 nm was higher than predicted by the fit in Fig. 3. We assume that this was due to imperfect constructive interference of up-converted (re-converted) light with the pumped cavity mode, but operation at these powers should in any case be avoided to retain a stable and well controllable system.

C. Interference of converted beams

In the next step, we duplicated the DOPO setup and measured the visibility between the two independently created light fields at 2128 nm. For this, the beams were overlapped on a 50/50 beam splitter. A piezo-mounted mirror allowed us to scan the relative phase between the two fields, cf. figure 1. The resulting interference fringes were monitored on a photodiode in one of the beam splitter output ports, see figure 4. We observed a stable and stationary interference pattern, indicating quasi-identical operation of the two DOPOs and high coherence between the two fields. A maximum interferometric visibility

$$V = \frac{I_{\max} - I_{\min}}{I_{\max} + I_{\min}} = 0.975$$

was achieved, where I_{\min} and I_{\max} are the light powers detected at the minimum and maximum of the interference fringe, respectively.

The visibility is a measure for the coherence properties of light. Deviations from $V = 1$ are furthermore caused by non-perfect beam overlap, differing beam powers, as well as phase and amplitude fluctuations [33]. Our measured visibility is the sum of all these imperfections, which results in an upper limit for the coherence properties of the converted fields. We assume that our visibility value was limited by imperfect beam overlap and even higher values would be achievable with careful alignment. We conclude that the two individual wavelength conversions preserve coherence properties to a high degree and therefore that the conversion approach is suitable for interferometric applications.

D. Power stability

Converting the wavelength should retain the stability properties of the pump beam, without introducing additional power drifts or amplitude noise. We measured the intensity of the pumped and converted

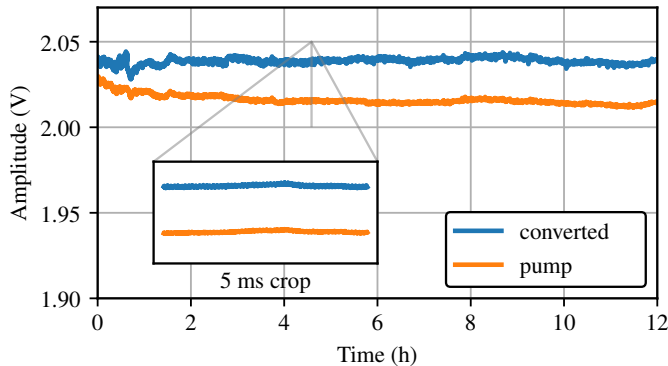


Fig. 5. Long and short term stability of the pumped and converted light. The first two hours show larger disturbances, which reduce after the optical setup has thermalized and traffic around the lab area reduced during the night. Note the scale on the y-axis.

light with separate photodiodes for twelve hours at a sampling rate of 200 kHz. Figure 5 shows the long and short term intensity stability, over the full time span and a zoom into a 5 ms segment. Both traces show small disturbances which are mostly correlated between both beams. The relative error margins, starting from a settling time of 3 hours, are 0.11 % (pump) and 0.15 % (converted). The overall stability of the 2 μm light is thus similar to the stability of the NPRO pump laser.

4. CONCLUSION

We have reported on a stable, coherent light source at 2128 nm using high-efficiency degenerate optical-parametric oscillation. We showed long-term stability over many hours and proved strong coherence between two individually converted fields, with a measured visibility of $V = 0.975$.

While our setup was optimized for low pump powers, our obtained value for the non-linearity allows for the conversion maximum to be adapted to arbitrary powers, by changing the reflectivities of the DPOPO mirrors. Our approach should thus enable the conversion of the highly stable 1064 nm lasers used in current gravitational-wave detectors with powers above 100 W with external conversion efficiencies greater 80 %. Furthermore, our scheme can be readily extended to create squeezed states of light, which have become an integral part of all current and future gravitational-wave detectors.

Funding Information. This research has been funded by the Deutsche Forschungsgemeinschaft (DFG, German Research Foundation) – 388405737. This article has LIGO document number P2000265 and Virgo codifier VIR-0668A-20.

Disclosures. The authors declare no conflicts of interest.

REFERENCES

1. B. P. Abbott and et al., Phys. Rev. Lett. **116** (2016).
2. LIGO Scientific Collaboration and Virgo Collaboration, Phys. Rev. Lett. **119**, 161101 (2017).
3. LIGO Scientific Collaboration and Virgo Collaboration, The Astrophys. J. **896**, L44 (2020).
4. D. Shoemaker, "Gravitational-Wave Astronomy in the 2020s and Beyond: A View Across the Gravitational Wave Spectrum," Tech. rep. (2019).
5. Y. Levin, Phys. Rev. D **57**, 659 (1998).

6. G. M. Harry, A. M. Gretarsson, P. R. Saulson, S. E. Kittelberger, S. D. Penn, W. J. Startin, S. Rowan, M. M. Fejer, D. R. M. Crooks, G. Cagnoli, J. Hough, and N. Nakagawa, Class. Quantum Gravity **19**, 897 (2002).
7. L. Barsotti, S. Gras, M. Evans, and P. Fritschel, "The updated Advanced LIGO design curve," Tech. rep. (2018).
8. S. Hild, S. Chelkowski, A. Freise, J. Franc, N. Morgado, R. Flaminio, and R. DeSalvo, Class. Quantum Gravity **27**, 015003 (2010).
9. ET Science Team, "Einstein gravitational wave Telescope conceptual design study," (2011).
10. P. G. Murray, I. W. Martin, K. Craig, J. Hough, R. Robie, S. Rowan, M. R. Abernathy, T. Pershing, and S. Penn, Phys. Rev. D **92**, 062001 (2015).
11. J. Steinlechner, I. W. Martin, A. S. Bell, J. Hough, M. Fletcher, P. G. Murray, R. Robie, S. Rowan, and R. Schnabel, Phys. Rev. Lett. **120**, 263602 (2018).
12. LIGO Scientific Collaboration, "Instrument Science White Paper 2019," Tech. rep. (2019).
13. M. A. Green and M. J. Keevers, Prog. Photovoltaics: Res. Appl. **3**, 189 (1995).
14. ETpathfinder Team, "ETpathfinder Design Report," (2020).
15. R. Schnabel, N. Mavalvala, D. E. McClelland, and P. K. Lam, Nat. communications **1**, 121 (2010).
16. J. Abadie, E. al., and The LIGO Scientific Collaboration, Nat. Phys. **7**, 962 (2011).
17. M. Tse and et al., Phys. Rev. Lett. **123**, 231107 (2019).
18. F. Acernese and et al., Phys. Rev. Lett. **123**, 231108 (2019).
19. G. L. Mansell, T. G. McRae, P. A. Altin, M. J. Yap, R. L. Ward, B. J. J. Slagmolen, D. A. Shaddock, and D. E. McClelland, Phys. Rev. Lett. **120** (2018).
20. R. C. Eckardt, C. D. Nabors, W. J. Kozlovsky, and R. L. Byer, J. Opt. Soc. Am. B **8**, 646 (1991).
21. C. D. Nabors, S. T. Yang, T. Day, and R. L. Byer, JOSA B **7**, 815 (1990).
22. G. K. L. Wong, S. G. Murdoch, R. Leonhardt, J. D. Harvey, and V. Marie, Opt. Express **15**, 2947 (2007).
23. G. Arisholm, Ø. Nordseth, and G. Rustad, Opt. Express **12**, 4189 (2004).
24. A. Marandi, N. C. Leindecker, K. L. Vodopyanov, and R. L. Byer, Opt. Express **20**, 19322 (2012).
25. T. J. Kane and R. L. Byer, Opt. Lett. **10**, 65 (1985).
26. C. Darsow-Fromm, L. Dekant, S. Grebien, M. Schröder, R. Schnabel, and S. Steinlechner, Rev. Sci. Instruments **91**, 035114 (2020).
27. J. A. Zielińska, A. Zukauskas, C. Canalías, M. A. Noyan, and M. W. Mitchell, Opt. Express **25**, 1142 (2017).
28. A. Schönbeck, "Compact squeezed-light source at 1550 nm," Ph.D. thesis, Hamburg (2018).
29. J. Falk, IEEE J. Quantum Electron. **7**, 230 (1971).
30. A. V. Smith, J. J. Smith, and B. T. Do, arXiv:1607.03964 [physics] (2016).
31. J. A. Giordmaine and R. C. Miller, Phys. Rev. Lett. **14**, 973 (1965).
32. N. Lastzka, "Numerical modelling of classical and quantum effects in non-linear optical systems," PhD Thesis (2010).
33. O. Svelto and D. C. Hanna, *Principles of Lasers* (Springer, New York, 2010), 5th ed.

FULL REFERENCES

1. B. P. Abbott and et al., "Observation of Gravitational Waves from a Binary Black Hole Merger," *Phys. Rev. Lett.* **116** (2016).
2. LIGO Scientific Collaboration and Virgo Collaboration, "GW170817: Observation of Gravitational Waves from a Binary Neutron Star Inspiral," *Phys. Rev. Lett.* **119**, 161101 (2017).
3. LIGO Scientific Collaboration and Virgo Collaboration, "GW190814: Gravitational Waves from the Coalescence of a 23 Solar Mass Black Hole with a 2.6 Solar Mass Compact Object," *The Astrophys. J.* **896**, L44 (2020).
4. D. Shoemaker, "Gravitational-Wave Astronomy in the 2020s and Beyond: A View Across the Gravitational Wave Spectrum," *Tech. rep.* (2019).
5. Y. Levin, "Internal thermal noise in the LIGO test masses: A direct approach," *Phys. Rev. D* **57**, 659–663 (1998).
6. G. M. Harry, A. M. Gretarsson, P. R. Saulson, S. E. Kittelberger, S. D. Penn, W. J. Startin, S. Rowan, M. M. Fejer, D. R. M. Crooks, G. Cagnoli, J. Hough, and N. Nakagawa, "Thermal noise in interferometric gravitational wave detectors due to dielectric optical coatings," *Class. Quantum Gravity* **19**, 897–917 (2002).
7. L. Barsotti, S. Gras, M. Evans, and P. Fritschel, "The updated Advanced LIGO design curve," *Tech. rep.* (2018).
8. S. Hild, S. Chelkowski, A. Freise, J. Franc, N. Morgado, R. Flaminio, and R. DeSalvo, "A xylophone configuration for a third-generation gravitational wave detector," *Class. Quantum Gravity* **27**, 015003 (2010).
9. ET Science Team, "Einstein gravitational wave Telescope conceptual design study," (2011).
10. P. G. Murray, I. W. Martin, K. Craig, J. Hough, R. Robie, S. Rowan, M. R. Abernathy, T. Pershing, and S. Penn, "Ion-beam sputtered amorphous silicon films for cryogenic precision measurement systems," *Phys. Rev. D* **92**, 062001 (2015).
11. J. Steinlechner, I. W. Martin, A. S. Bell, J. Hough, M. Fletcher, P. G. Murray, R. Robie, S. Rowan, and R. Schnabel, "Silicon-Based Optical Mirror Coatings for Ultrahigh Precision Metrology and Sensing," *Phys. Rev. Lett.* **120**, 263602 (2018).
12. LIGO Scientific Collaboration, "Instrument Science White Paper 2019," *Tech. rep.*, LIGO Scientific Collaboration (2019).
13. M. A. Green and M. J. Keevers, "Optical properties of intrinsic silicon at 300 K," *Prog. Photovoltaics: Res. Appl.* **3**, 189–192 (1995).
14. ETpathfinder Team, "ETpathfinder Design Report," (2020).
15. R. Schnabel, N. Mavalvala, D. E. McClelland, and P. K. Lam, "Quantum metrology for gravitational wave astronomy," *Nat. communications* **1**, 121 (2010).
16. J. Abadie, E. al., and The LIGO Scientific Collaboration, "A gravitational wave observatory operating beyond the quantum shot-noise limit," *Nat. Phys.* **7**, 962–965 (2011).
17. M. Tse and et al., "Quantum-Enhanced Advanced LIGO Detectors in the Era of Gravitational-Wave Astronomy," *Phys. Rev. Lett.* **123**, 231107 (2019).
18. F. Acernese and et al., "Increasing the Astrophysical Reach of the Advanced Virgo Detector via the Application of Squeezed Vacuum States of Light," *Phys. Rev. Lett.* **123**, 231108 (2019).
19. G. L. Mansell, T. G. McRae, P. A. Altin, M. J. Yap, R. L. Ward, B. J. J. Slagmolen, D. A. Shaddock, and D. E. McClelland, "Observation of Squeezed Light in the 2 Mm Region," *Phys. Rev. Lett.* **120** (2018).
20. R. C. Eckardt, C. D. Nabors, W. J. Kozlovsky, and R. L. Byer, "Optical parametric oscillator frequency tuning and control," *J. Opt. Soc. Am. B* **8**, 646 (1991).
21. C. D. Nabors, S. T. Yang, T. Day, and R. L. Byer, "Coherence properties of a doubly resonant monolithic optical parametric oscillator," *JOSA B* **7**, 815–820 (1990).
22. G. K. L. Wong, S. G. Murdoch, R. Leonhardt, J. D. Harvey, and V. Marie, "High-conversion-efficiency widely-tunable all-fiber optical parametric oscillator," *Opt. Express* **15**, 2947–2952 (2007).
23. G. Arisholm, Ø. Nordseth, and G. Rustad, "Optical parametric master oscillator and power amplifier for efficient conversion of high-energy pulses with high beam quality," *Opt. Express* **12**, 4189–4197 (2004).
24. A. Marandi, N. C. Leindecker, K. L. Vodopyanov, and R. L. Byer, "All-optical quantum random bit generation from intrinsically binary phase of parametric oscillators," *Opt. Express* **20**, 19322–19330 (2012).
25. T. J. Kane and R. L. Byer, "Monolithic, unidirectional single-mode Nd:YAG ring laser," *Opt. Lett.* **10**, 65 (1985).
26. C. Darsow-Fromm, L. Dekant, S. Grebien, M. Schröder, R. Schnabel, and S. Steinlechner, "NQontrol: An open-source platform for digital control-loops in quantum-optical experiments," *Rev. Sci. Instruments* **91**, 035114 (2020).
27. J. A. Zielińska, A. Zukauskas, C. Canalias, M. A. Noyan, and M. W. Mitchell, "Fully-resonant, tunable, monolithic frequency conversion as a coherent UVA source," *Opt. Express* **25**, 1142–1150 (2017).
28. A. Schönbeck, "Compact squeezed-light source at 1550 nm," *Ph.D. thesis*, Universität Hamburg, Hamburg (2018).
29. J. Falk, "Instabilities in the doubly resonant parametric oscillator: A theoretical analysis," *IEEE J. Quantum Electron.* **7**, 230–235 (1971).
30. A. V. Smith, J. J. Smith, and B. T. Do, "Thermo-optic and thermal expansion coefficients of RTP and KTP crystals over 300-350 K," *arXiv:1607.03964 [physics]* (2016).
31. J. A. Giordmaine and R. C. Miller, "Tunable Coherent Parametric Oscillation in LiNbO₃ at Optical Frequencies," *Phys. Rev. Lett.* **14**, 973–976 (1965).
32. N. Lastzka, "Numerical modelling of classical and quantum effects in non-linear optical systems," *PhD Thesis*, Universität Hannover (2010).
33. O. Svelto and D. C. Hanna, *Principles of Lasers* (Springer, New York, 2010), 5th ed.